

# NEURAL IMAGE-BASED AVATARS: GENERALIZABLE RADIANCE FIELDS FOR HUMAN AVATAR MODELING

**Youngjoong Kwon<sup>1</sup>, Dahun Kim<sup>2</sup>, Duygu Ceylan<sup>3</sup>, Henry Fuchs<sup>1</sup>**

<sup>1</sup>University of North Carolina at Chapel Hill. <sup>2</sup>Google Research, Brain Team. <sup>3</sup>Adobe Research.  
`{youngjoong, fuchs}@cs.unc.edu` `{mcahny}@google.com` `{ceylan}@adobe.com`

## ABSTRACT

We present a method that enables synthesizing novel views and novel poses of arbitrary human performers from sparse multi-view images. A key ingredient of our method is a hybrid appearance blending module that combines the advantages of the implicit body NeRF representation and image-based rendering. Existing generalizable human NeRF methods that are conditioned on the body model have shown robustness against the geometric variation of arbitrary human performers. Yet they often exhibit blurry results when generalized onto unseen identities. Meanwhile, image-based rendering shows high-quality results when sufficient observations are available, whereas it suffers artifacts in sparse-view settings. We propose Neural Image-based Avatars (NIA) that exploits the best of those two methods: to maintain robustness under new articulations and self-occlusions while directly leveraging the available (sparse) source view colors to preserve appearance details of new subject identities. Our hybrid design outperforms recent methods on both in-domain identity generalization as well as challenging cross-dataset generalization settings. Also, in terms of the pose generalization, our method outperforms even the per-subject optimized animatable NeRF methods. The video results are available at <https://youngjoongc.github.io/nia>.

## 1 INTRODUCTION

Acquisition of 3D renderable full-body avatars is critical for applications to virtual reality, telepresence and human modeling. While early solutions have required heavy hardware setups such as dense camera rigs or depth sensors, recent neural rendering techniques have achieved significant progress to a more scalable and low-cost solution. Notably, neural radiance fields (NeRF) based methods facilitated by the parametric body prior Loper et al. (2015) require only sparse camera views to enable visually pleasing free-view synthesis Peng et al. (2021b); Kwon et al. (2021); Zhao et al. (2022); Cheng et al. (2022) or pose animation Peng et al. (2021a); Su et al. (2021) of the human avatar.

Still, creating a full-body avatar from sparse images (*e.g.*, three snaps) of a person is a challenging problem due to the complexity and diversity of possible human appearances and poses. Most existing methods Peng et al. (2021b;a) are therefore focusing on person-specific setting which requires a dedicated model optimization for each new subject it encounters. More recent methods explore generalizable human NeRF representations Peng et al. (2021b); Raj et al. (2021b); Kwon et al. (2021); Zhao et al. (2022) by using pixel-aligned features in a data-driven manner. Among them, Kwon et al. (2021) and Chen et al. (2022) specifically exploit the *body surface feature* conditioned NeRF (*i.e.*, pixel-aligned features anchored at the SMPL vertices) which helps robustness to various articulations while obviating the need for the 3D supervision Zhao et al. (2022); Cheng et al. (2022). Nevertheless, these body surface feature conditioned NeRFs still suffer blur artifacts when generalizing onto unseen subject identities with complex poses. Also, an extra effort on video-level feature aggregation is required in Kwon et al. (2021) to compensate for the sparsity of input views.

In this paper, we propose Neural Image-based Avatars (NIA) that generalizes novel view synthesis and pose animation for arbitrary human performers from a sparse set of still images. It is a hybrid framework that combines body surface feature conditioned NeRF (*e.g.*, Kwon et al. (2021)) and image-based rendering techniques (*e.g.*, Wang et al. (2021)). While the former helps in robust representation of different body shapes and poses, the image-based rendering helps preserving the

color and texture details from the source images. This can complement the NeRF predicted colors which are often blur and inaccurate in generalization settings (cross-identity as well as cross-dataset generalization) as shown in Fig. 2 and Fig. 5. To leverage the best of both worlds, we propose a neural appearance blending scheme that learns to adaptively blend the NeRF predicted colors with the direct source image colors. Last but not least, by deforming the learned NIA representation based on the skeleton-driven transformations Lewis et al. (2000); Kavan et al. (2007), we enable plausible pose animation of the learned avatar.

To demonstrate the efficacy of our NIA method, we experiment on ZJU-MoCap Peng et al. (2021b) and MonoCap Habermann et al. (2020; 2021) datasets. First, experiments show that our method outperforms the state-of-the-art Neural Human Performer Kwon et al. (2021) and GP-NeRF Chen et al. (2022) in novel view synthesis task. Furthermore, we study the more challenging cross-dataset generalization by evaluating the zero-shot performance on the MonoCap Habermann et al. (2020; 2021) datasets, where we clearly outperform the previous methods. Finally, we evaluate on the pose animation task, where our NIA tested on *unseen subjects* achieves better pose generalization than the *per-subject* trained A-NeRF Su et al. (2021) and Animatable-NeRF Peng et al. (2021a) that are tested on the *seen* training subjects. The ablation studies demonstrate that the proposed modules of our NIA collectively contribute to the high-quality rendering for arbitrary human subjects.

## 2 RELATED WORK

Combined with Neural Radiance Fields (NeRF) Mildenhall et al. (2020), human reconstruction research has shown unprecedented development Pumarola et al. (2020); Park et al. (2021a;b). Human priors are utilized to enable robust reconstruction of face and body Gao et al. (2020); Gafni et al. (2021); Peng et al. (2021b). However, these methods are per-subject optimized, and cannot model the motions that are not seen during training. Therefore, subsequent works have been focusing on generalization in two directions: pose and subject identity.

**Pose generalization.** Su et al. (2021) utilize a joint-relative encoding for dynamic articulations. Noguchi et al. (2021) explicitly associate 3D points to body parts. Chen et al. (2021) and Peng et al. (2021a) deform the target pose space queries into the canonical space to obtain the color and density values. Liu et al. (2021) leverages normal map as the dense pose cue. Xu et al. (2021) learns deformable signed distance field. Weng et al. (2022) and Peng et al. (2022) decompose the human deformation into articulation-driven and non-rigid deformations. Su et al. (2022) and Zheng et al. (2022) utilize the joint-specific local radiance fields. Despite the significant progress in pose generalization, they still focus on a subject-specific setting which requires training a single model for each subject. In this paper, we tackle generalization across both poses and subject identities.

**Subject identity generalization.** The use of image-conditioned Rebain et al. (2022) or pixel-aligned features Yu et al. (2020); Wang et al. (2021) has allowed generalized neural human representations from sparse camera views. Raj et al. (2021b) use camera-encoded pixel-aligned features for face view synthesis. Kwon et al. (2021) aggregate temporal features by anchoring them onto the SMPL body vertice to complement the sparse input views. Chen et al. (2022) also leverages body surface features to enable full-body synthesis. Zhao et al. (2022) and Cheng et al. (2022) also propose the neural blending of NeRF prediction with source view colors. Specifically, they use the pixel-aligned features-conditioned NeRF as their implicit body representation. However, pixel-aligned features alone are prone to errors under complex poses as reported in Kwon et al. (2021). Therefore, their method require 3D supervision (*e.g.*, depth, visibility) or per-subject finetuning. In contrast to these methods, we aim at generalizing human modeling without relying on the 3D supervision or per-subject finetuning, but by using only RGB supervision.

**Other non NeRF-based methods.** Deferred neural rendering based methods Thies et al. (2019); Raj et al. (2021a); Grigorev et al. (2021) enable fast synthesis of person-specific avatar by combining the traditional graphics pipeline with the neural texture maps. Grigorev *et al.* further finetunes to deal with unseen subjects. In contrast, we focus on the generalization without any finetuning. Kwon et al. (2020b;a) exploit volumetric representations to enable free view synthesis from a few snapshots of unseen subjects. Saito et al. (2019; 2020); He et al. (2021) leverage pixel-aligned features to enable 3d reconstruction from a single image, while requiring 3D groundtruth supervision. Habermann et al. (2019); Liu et al. (2020); Habermann et al. (2021); Bagautdinov et al. (2021) generate high-quality non-rigid deformation, but they require the template mesh optimization. Aliev et al. (2019); Wu et al.

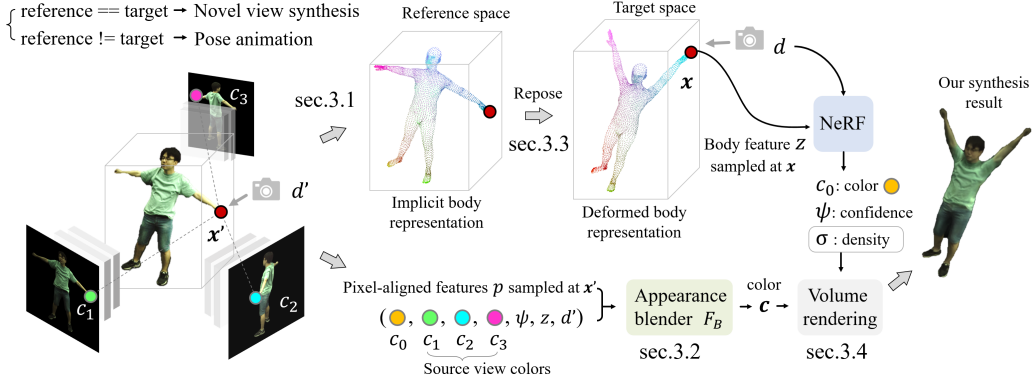


**Figure 1: Overview of Neural Image-based Avatars (NIA) method.** Given a sparse view images of an unseen person in the reference space, NIA instantly creates a human avatar for novel view synthesis and pose animation. NIA is a hybrid approach combining the SMPL-based implicit body representation and the image-based rendering method. Our appearance blender learns to adaptively blend the predictions from the two components. Note that if the reference space and the target pose spaces are identical (*i.e.*, no pose difference,  $x = x'$ ,  $d = d'$ ), the task is novel view synthesis. Otherwise, it is a pose animation task where we deform the NIA representation to repose the learned avatar.

(2020) anchor features on the point clouds and render them with differentiable rasterizer. However, they require sufficient amount of point clouds that cannot be obtained from our sparse input view setting. In this work, we mainly focus on and compare with the NeRF-based methods.

### 3 METHOD

The overview of our NIA is given in Fig. 1. Our goal is to obtain a Neural Image-based Avatars (NIA) which after training, can directly synthesize novel views and novel poses of an unseen person in a feed-forward manner from very sparse input views. To deal with complex and diverse human appearances and poses, we propose a *hybrid* framework that leverages the advantages of two representations. The first is a neural radiance fields based body representation conditioned on a parametric human model (SMPL Loper et al. (2015)), which can provide the body geometry and pose-dependent deformations (Sec. 3.1). Inspired by Wang et al. (2021), the second is obtained by neural image-based rendering which can improve the fine-details of the result by directly fetching the pixel colors from the source view images. A core of our design is a neural appearance blending scheme that learns to blend predictions from the two representations and outputs the final synthesis results (Sec. 3.2). Given a set of sparse view images of an arbitrary person, our learned NIA not only performs novel view synthesis, but also reposing by deforming the representation of the avatar at capture time into the desired target pose (Sec. 3.3).

We note that we assume the calibration parameters of the multi-view input images and the foreground human region masks are known, and the fitted SMPL models are available.

#### 3.1 BASELINE: GENERALIZABLE IMPLICIT BODY REPRESENTATION

Inspired by NHP Kwon et al. (2021) and GP-NeRF Chen et al. (2022), our implicit body NeRF representation follows the design of body surface feature conditioned NeRF (*i.e.*, pixel-aligned features anchored at SMPL vertices).

Given  $N$  available source views, we extract pixel-aligned image features Saito et al. (2019) from each view  $n$  and attach them to the SMPL vertices, to construct a per-view coarse feature set  $P_n$ . Each vertex location is projected to the image feature plane and the corresponding pixel-aligned feature is computed by bilinearly interpolating the grid pixel values. Since  $P_n$  is sparse in 3D to represent the whole human body, we use 3D sparse convolutions Liu et al. (2015) to diffuse the features into a denser feature volume. The sparse convolutions learn to extrapolate the sparse feature points  $P_n$  to build a dense body feature volume  $\tilde{P}_n$  that better adapts to the target body shape. For each query

point  $\mathbf{x}$ , we sample the corresponding body feature from  $\tilde{P}_n$ . The sampled features from  $N$  source views are then processed by a view-wise cross-attention with the pixel-aligned features to obtain the multi-view aware body feature  $\mathbf{z}_n$ . Besides the final density  $\sigma$  and color value  $\mathbf{c}_0$ , we also propose to predict the confidence  $\psi \in [0, 1]$  of its color prediction as:

$$\sigma = F_\sigma \left( \sum_n \mathbf{z}_n / N \right), \quad \mathbf{c}_0, \psi, \mathbf{h} = F_{\mathbf{c}_0} \left( \sum_n (\mathbf{z}_n; \gamma(d)) / N \right), \quad (1)$$

where  $F_\sigma$  and  $F_{\mathbf{c}_0}$  are MLPs consisting of four linear layers respectively, and  $\gamma : \mathbb{R}^{3 \times 6 \times l} \rightarrow \mathbb{R}^{3 \times 6 \times l}$  is a positional encoding of viewing direction  $d \in \mathbb{R}^3$  as in Mildenhall et al. (2020) with  $2 \times l$  different basis functions.  $\mathbf{h}$  is the intermediate color feature extracted from the second to last layer of  $F_{\mathbf{c}_0}$  that is later used in the appearance blending (Sec. 3.2).

### 3.2 LEARNABLE APPEARANCE BLENDING

While our implicit body NeRF representation helps in robustness to geometric variation of arbitrary human shapes, it is difficult for such a general NeRF representation to convey all the high-frequency details (color and textures) present in the source view images. To remedy this, we leverage ideas from image-based rendering techniques Chen & Williams (1993); Buehler et al. (2001); Gortler et al. (1996); Levoy & Hanrahan (1996); Debevec et al. (1998); Hedman et al. (2018); Wang et al. (2021). In particular, a query point  $\mathbf{x}$  can be projected to  $N$  source views to directly retrieve the color values. We propose an appearance blending module  $F_B$  that learns to predict blending weights among the  $N$  source view colors  $\mathbf{c}_n$  and the NeRF generated color  $\mathbf{c}_0$ .

The inputs to this network are the pixel-aligned features  $p_n$  for  $\mathbf{x}$ , the relative viewing direction  $\hat{d}_n$  which is defined by the difference and dot product between the target viewing direction  $d$  and the source viewing direction  $d_n$ , the visibility  $o_n$  of  $\mathbf{x}$  with respect to each source view, the intermediate NeRF color feature  $\mathbf{h}$  and the color confidence  $\psi$  from  $F_{\mathbf{c}_0}$ . We define the view index for the implicit body NeRF representation as  $n=0$ . Formally, the blending weights  $w_n^{rgb}$  are computed as:

$$\{w_n^{rgb}\}_{n=0}^N = F_B(\{p_n; \hat{d}_n; o_n\}_{n=1}^N, \mathbf{h}, \psi). \quad (2)$$

Note that our visibility  $o_n$  is computed *without* the need for any ground truth 3D geometry. To pursue our scalable and practical setting without the reliance on the 3D supervision, we propose to exploit the underlying parametric body model to approximate the visibility for each query point. Specifically, we borrow the vertex visibility of the SMPL model. As in Huang et al. (2020); Bhatnagar et al. (2020); Peng et al. (2021a), we first search the SMPL mesh surface that is closest to the query point. Then, we define the visibility as a float value  $o_n \in [0, 1]$  computed by the barycentric interpolation of the 0-or-1 visibility values of three vertices on the corresponding mesh facet. This is different from Cheng et al. (2022), where visibility trained with groundtruth is required. Also, our design differs from Zhao et al. (2022), where the groundtruth-supervised depth is utilized to sample source view colors. The final color  $\mathbf{c}$  for  $\mathbf{x}$  is computed via softmax as  $\mathbf{c} = \sum_{n=0}^N (\exp(w_n^{rgb}) \mathbf{c}_n) / (\sum_{i=0}^N \exp(w_i^{rgb}))$ .

### 3.3 RE-POSING NIA FOR POSE ANIMATION

We describe how our proposed NIA can be extended to animate an unseen subject given new target poses at inference without any further training. Different from the previous works Chen et al. (2021); Peng et al. (2021a; 2022), where a canonical feature space for appearance retrieval is optimized in a per-subject manner, our generalization approach aims at reposing the NIA avatars that are created on the fly given a set of sparse reference images of unseen human subjects. Since the available source images in the reference space cannot be directly used in the target pose space (*i.e.*, observation space), the construction of our NIA representations should be considered with the deformation between the target and reference spaces.

To build the implicit body feature volume in the target pose space, we retrieve the relevant pixel-aligned features from the location of the reference SMPL vertices. By using the known SMPL correspondences, these pixel-aligned feature points are relocated and attached to the corresponding target pose SMPL vertices. The following sparse convolutions will result in the feature volume in the target pose space, where each body feature  $z_n^{tar}$  is sampled from. The density and color in the target space are computed similarly to Eq. (1), except we use  $z_n^{tar}$  that is transformed into the reference space, instead of  $z_n$ .

The appearance blending is defined similarly to Eq. (2) using the target-to-reference transformed query location  $\mathbf{x}'$  and viewing direction  $d'$ , instead of  $\mathbf{x}$  and  $d$ . The visibility is computed with respect to  $\mathbf{x}'$  and the reference SMPL body.

**Deformation modeling.** We model the deformation  $T$  from the target pose space (observation space) to reference space as the skeleton-driven deformation, which is the composition of the inverse and forward linear-blend skinning Lewis et al. (2000). Specifically, we can transform the query  $\mathbf{x}$  in the target space into the reference space location  $\mathbf{x}'$  through  $T(\mathbf{x}) = (T^{fwd} \circ T^{inv})(\mathbf{x})$ , where  $T^{inv}$  and  $T^{fwd}$  are defined as:

$$T^{inv} = \left( \sum_{k=1}^K w_k^{tar}(\mathbf{x}) G_k \right)^{-1} \mathbf{x} = \mathbf{x}^{can}, \quad T^{fwd} = \left( \sum_{k=1}^K w_k^{can}(\mathbf{x}^{can}) G_k \right)^{-1} \mathbf{x}^{can} = \mathbf{x}', \quad (3)$$

where  $\{G_k\} \in SE(3)$  is the  $K$  transformation matrices produced by SMPL skeleton with  $K$  body parts, and  $w_k^{tar}$  and  $w_k^{can}$  are the blending weights for  $k$ -th part sampled in the target and canonical space, respectively. Similar to the visibility computation (Sec. 3.2), the blending weight is interpolated from the blending weights of the nearest SMPL vertices.

The deformation  $\tilde{T}$  for the viewing direction, which transforms the target-space viewing direction  $\mathbf{d}$  to the reference space viewing direction  $\mathbf{d}'$  is defined in a similar manner. We denote the weighted sum of transformation matrices of  $T$  as  $[R(\mathbf{x}); t(\mathbf{x})]$ . Then,  $\tilde{T}(\mathbf{d})$  is defined as  $\tilde{T}(\mathbf{d}) = R(\mathbf{x})\mathbf{d} = \mathbf{d}'$ .

### 3.4 VOLUME RENDERING AND LOSS FUNCTION

**Volume rendering.** To decide the color of each ray, we accumulate the density and color predictions along the ray  $\mathbf{r}(t) = \mathbf{r}_0 + t\mathbf{d}$  for  $t \in [t_{near}, t_{far}]$  as defined in NeRF Mildenhall et al. (2020) as follows:

$$\mathbf{C}(r) = \int_{t_{near}}^{t_{far}} \mathbf{T}(t)\sigma(\mathbf{r}(t))\mathbf{c}(\mathbf{r}(t), \mathbf{d})dt, \quad \text{where} \quad \mathbf{T}(t) = \exp \left( - \int_{t_{near}}^t \sigma(\mathbf{r}(s))ds \right) \quad (4)$$

In practice, we uniformly sample a set of 64 points  $t \sim [t_{near}, t_{far}]$ . The bounds for ray sampling  $t_{near}, t_{far}$  are driven by computing the 3D bounding box of the SMPL body.

**Loss function.** Together with the final blended appearance  $\mathbf{c}$ , we also supervise the NeRF regressed  $\mathbf{c}_0$  with a simple photometric loss to improve the prediction quality:  $\mathcal{L} = \|\mathbf{c}_0 - \hat{\mathbf{c}}\|_2 + \|\mathbf{c} - \hat{\mathbf{c}}\|_2$  where  $\hat{\mathbf{c}}$  denotes the groundtruth pixel color.

## 4 EXPERIMENTAL RESULTS

To demonstrate the effectiveness of our proposed NIA method, we conduct experiments for novel view synthesis and pose animation tasks. We use ZJU-MoCap Peng et al. (2021b) for both tasks and ablation studies. Then we study our cross-dataset generalization ability by training on ZJU-Mocap and testing on MonoCap datasets without any finetuning.

### 4.1 IDENTITY GENERALIZATION

**Competing baselines.** For novel view synthesis, the state-of-the-art competitors are NHP Kwon et al. (2021) and GP-NeRF Chen et al. (2022) which robustly perform generalization with the body surface feature. Other generalizable methods are pixel-NeRF Yu et al. (2020), PVA Raj et al. (2021b), Image-Based Rendering Network (IBRNet) Wang et al. (2021), and Keypoint NeRF Mihajlovic et al. (2022). We also compare with per-subject optimization method Neural Body Peng et al. (2021b), Neural Textures (NT) Thies et al. (2019), and Neural Human Rendering (NHR) Wu et al. (2020).

For pose animation task, we compare with the per-subject animatable NeRF methods which are Neural Body Peng et al. (2021b), A-NeRF Su et al. (2021) and Animatable-NeRF Peng et al. (2021a).

Note that the comparison with per-subject methods in both tasks is for reference purpose and places our (and other) generalizable method in disadvantage. These methods require one model (network) trained for a single subject, *i.e.*, as many models as the number of testing subjects, and they are

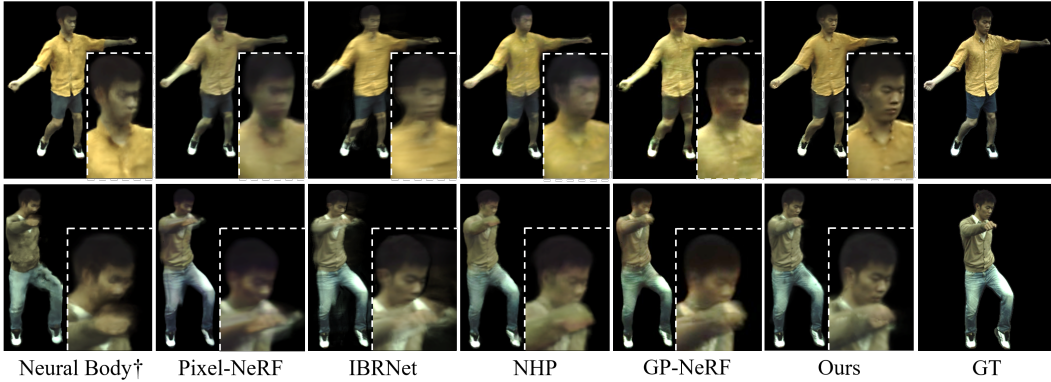


Figure 2: Novel view synthesis results on ZJU-MoCap dataset. †: Neural Body Peng et al. (2021b) is a per-subject optimized method, and is tested on the seen subjects with unseen poses. Pixel-NeRF Yu et al. (2020), IBRNet Wang et al. (2021), NHP Kwon et al. (2021) and GP-NeRF Chen et al. (2022) are generalizable methods which are tested on unseen subjects with unseen poses.

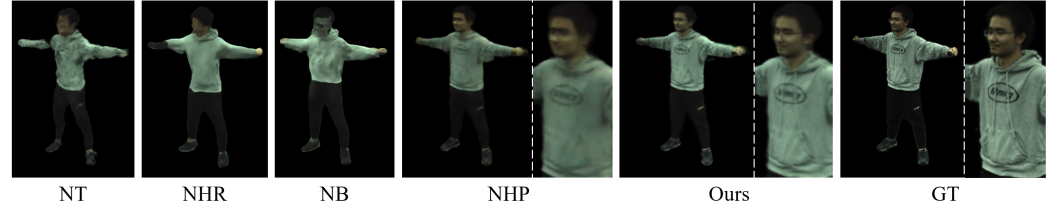


Figure 3: Results on the unseen poses of seen subjects on ZJU-MoCap dataset. NT: Neural Texture Thies et al. (2019), NHR: Multi-view Neural Human Rendering Wu et al. (2020), NB: Neural Body Peng et al. (2021b), NHP: Neural Human Performer Kwon et al. (2021), and NIA (ours). NT, NHR, NB are per-subject optimized methods.

| method                         | PSNR         | SSIM          |
|--------------------------------|--------------|---------------|
| <b>Training: per-subject</b>   |              |               |
| NT                             | 22.28        | 0.8720        |
| NHR                            | 22.31        | 0.8710        |
| NB                             | 23.79        | 0.8870        |
| <b>Training: generalizable</b> |              |               |
| NHP                            | 26.94        | 0.9290        |
| <b>NIA (ours)</b>              | <b>27.57</b> | <b>0.9398</b> |

| method            | PSNR         | SSIM          |
|-------------------|--------------|---------------|
| PVA               | 23.15        | 0.8663        |
| Pixel-NeRF        | 23.17        | 0.8693        |
| IBRNet            | 24.54        | 0.8935        |
| NHP               | 24.75        | 0.9058        |
| GP-NeRF           | 24.49        | 0.9012        |
| Keypoint NeRF     | 25.03        | 0.8969        |
| <b>NIA (ours)</b> | <b>25.79</b> | <b>0.9200</b> |

a. Eval. on **seen** subjects, unseen poses.

b. Training: **generalizable** (*one model for multiple subjects*); Eval. on **unseen** subjects, unseen poses.

Table 1: Novel view synthesis on ZJU-MoCap. All are evaluated on the same testing sequences.

evaluated on the training seen subjects with unseen poses. On the other hand, the generalizable methods train only one model which is evaluated on all unseen subjects with unseen poses.

#### 4.1.1 NOVEL VIEW SYNTHESIS

**Setup.** The ZJU-MoCap dataset contains 10 human subjects with 23 synchronized cameras. We follow the same training and testing protocols as in Kwon et al. (2021).

**Results.** The quantitative comparison of our NIA and other methods is shown in Table. 1. Our model achieves state-of-the-art performance on ZJU-Mocap dataset. Especially, the previous state-of-the-art NHP Kwon et al. (2021) relies on temporally aggregated features to compensate the sparse input views. Our NIA outperforms NHP by +1.0 dB PSNR and +1.5% SSIM, while utilizing only

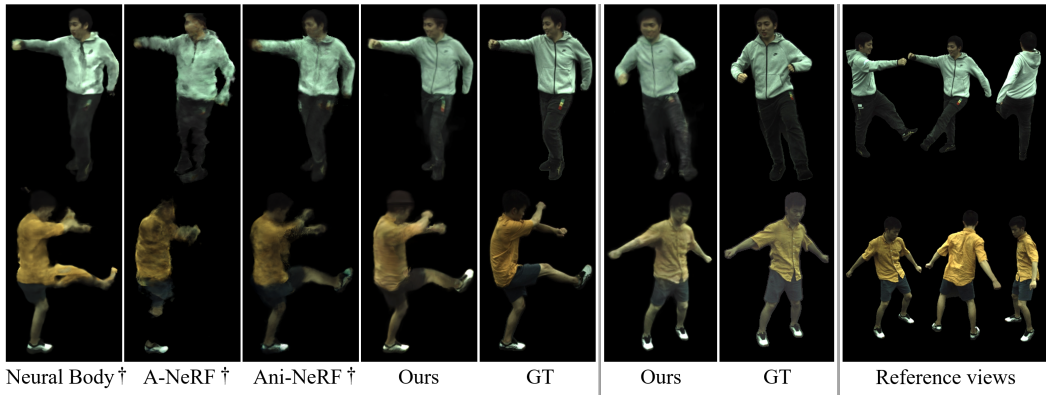


Figure 4: Pose animation results on ZJU-MoCap dataset. †: Neural Body Peng et al. (2021b), A-NeRF Su et al. (2021), and Ani-NeRF Peng et al. (2021a) are per-subject optimized methods, and are evaluated in novel pose synthesis for the seen subjects. Our NIA is the only generalizable method, and is evaluated in novel pose synthesis given only three-view reference images of unseen subjects. Column 6 and 7 are our results for another poses, and the ground truths. The last columns are the reference image input to our NIA.

still images. NIA also outperforms the most recent state-of-the-art methods GP-NeRF Chen et al. (2022) and Keypoint NeRF Mihajlovic et al. (2022) by +1.3 / +0.7 dB PSNR and +2.0 / +2.5% SSIM.

In Table. 1 and Fig. 3, we show the performance on the unseen poses of the seen subjects. Despite of the disadvantageous generalizable setting (one network for all subjects), our method significantly outperforms other baselines including the per-subject optimized methods.

As shown in Fig. 2, our NIA exhibits more high-frequency details compared to NHP and GP-NeRF. Other generalizable methods that utilize image-conditioned features (pixel-NeRF, PVA, and IBRNet) often suffer noisy surface prediction, while NIA shows more robust results on different human shapes.

#### 4.1.2 POSE ANIMATION

**Setup.** We evaluate our NIA for pose animation task on ZJU-MoCap dataset. Given a set of sparse view reference images of an unseen person, our on-the-fly generated avatar for that person is reposed to new target poses. We also use three input views for this task.

While we do perform generalization onto unseen subject identities, we compare with per-subject methods. Note that this comparison puts our method on *disadvantage* and thus is only to provide a reference level, since the competing methods have *seen* the testing subjects (no identity generalization for baselines).

Specifically, we compare with Neural Body Peng et al. (2021b), A-NeRF Su et al. (2021) and Animatable-NeRF Peng et al. (2021a) which made their code public and reported their results on ZJU-MoCap dataset. Meanwhile, we acknowledge there are more recent and advanced per-subject animation methods Su et al. (2022); Zheng et al. (2022); Peng et al. (2022); Weng et al. (2022). For all methods, we evaluate on the same testing sequences as in the novel view synthesis task.

**Results.** Table. 2 shows the quantitative comparison. Remarkably, our NIA model that is generalized onto unseen subjects outperforms the per-subject optimized competitors tested on seen subjects by healthy margins: +1.2 dB / +2.0% over Neural Body, +0.1 dB / +1.2% over A-NeRF and +0.1 dB / +1.1% over Animatable-NeRF in PSNR and SSIM, respectively. In Fig. 4, we observe that both Neural Body and Animatable-NeRF produce noisy and blurry texture output on novel poses, even though their models are trained to memorize the appearance of the same human subject. Our NIA method preserves relatively more high-frequency details like clothes wrinkles and textures. Note that it is a very challenging setting that requires our model to instantly create animatable avatars on the fly from only three reference view images of unseen human subjects.

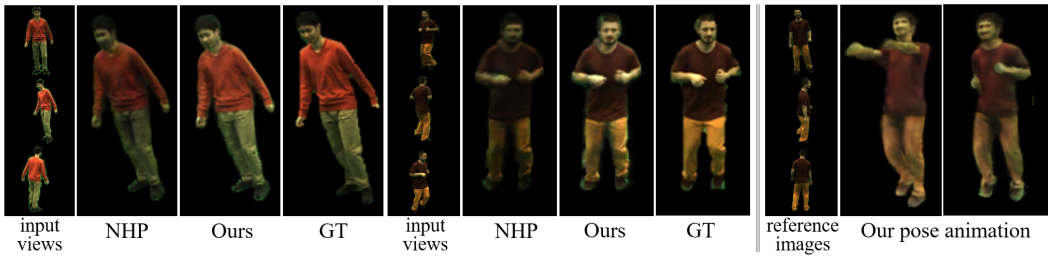


Figure 5: Cross-dataset generalization results without finetuning. Our NIA outperforms NHP Kwon et al. (2021) on novel view synthesis, when trained on ZJU-MoCap and tested on MonoCap datasets (left). Our NIA can also perform pose animation of unseen subjects given only a sparse set of still images (right).

| method            | training      | evaluation                       | PSNR         | SSIM          |
|-------------------|---------------|----------------------------------|--------------|---------------|
| Neural Body       |               |                                  | 22.88        | 0.8800        |
| A-NeRF            | per-subject   | seen subjects,<br>unseen poses   | 23.91        | 0.8893        |
| Animatable-NeRF   |               |                                  | 23.88        | 0.8901        |
| <b>NIA (ours)</b> | generalizable | unseen subjects,<br>unseen poses | <b>24.04</b> | <b>0.9000</b> |

Table 2: Pose animation on ZJU-MoCap dataset. All methods are evaluated on the same testing sequences and target poses. A-NeRF Su et al. (2021), Animatable-NeRF Peng et al. (2021a), and Ours.

| method            | PSNR         | SSIM          |
|-------------------|--------------|---------------|
| NHP               | 17.51        | 0.7457        |
| <b>NIA (ours)</b> | <b>19.12</b> | <b>0.7804</b> |

Table 3: Cross-dataset generalization (train on ZJU-MoCap, and test on MonoCap).

#### 4.2 CROSS-DATASET GENERALIZATION

For the out-of-domain, cross-dataset generalization, we train a model on the ZJU-MoCap dataset, and test on the MonoCap dataset without any finetuning. MonoCap consists of DeepCap Habermann et al. (2020) and DynaCap Habermann et al. (2021) dataset sequences that are captured by dense camera views. Given the different lighting and capture settings between the ZJU-MoCap and MonoCap datasets (*e.g.*, dark v. bright studio), our NIA improves the cross-dataset generalization over NHP by clear margins of +1.6 dB PSNR and +4.5 % SSIM in Table. 3.

As shown in the visual results (Fig. 5), the implicit body NeRF prediction of NHP especially suffers from the different color distribution between these datasets.

On the other hand, our NIA is a hybrid model combining the implicit body NeRF with the direct pixel fetching from the input images (*i.e.* image-based rendering), which helps to generalize to out-of-domain MonoCap datasets. Given only three snaps of a new person, our NIA is able to perform plausible pose animation as shown in Fig. 5 (right: ‘pose animation’).

#### 4.3 ABLATION STUDIES AND ANALYSIS

We provide ablation studies on ZJU-MoCap dataset by evaluating novel view synthesis performance of our NIA variants on unseen subject identities with unseen poses.

**NIA architecture designs.** We study the contribution of different modules of our NIA network in Table. 4.i and Fig. 6. First, we ablate the two main components of our method: implicit body representation (*a*) and image-based rendering (*b*). By removing each component, we observe a performance drop of -1.63 dB / -3.80% (*a*) and -1.55 dB / -1.49% (*b*) in PSNR and SSIM respectively. Fig. 6 visualizes how each component contributes to the rendering quality. Without the implicit body representation, the model tends to suffer inaccurate shape prediction especially on the regions fully occluded from all source views (*e.g.*, ghosting artifact near the right hand). On the other hand, removing the image-based rendering leads to blurry results and the loss of high-frequency texture details. Our full NIA model-(*e*) leverages these complementary merits and shows the best results both quantitatively and qualitatively.

We further investigate the impact of our neural appearance blending module. It learns to blend predictions from the implicit body representation (*i.e.* NeRF-predicted color) and the color values

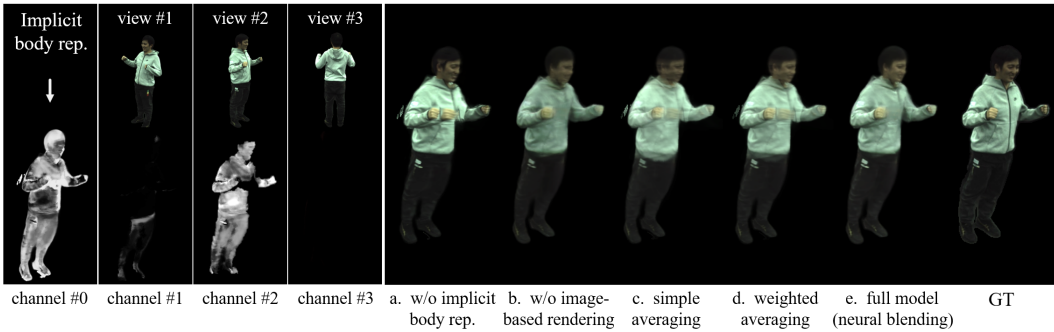


Figure 6: Input views (#1,2,3) and the corresponding channels of learned neural blending weight maps. Channel #0 corresponds to the prediction from the implicit body representation (NeRF). Remaining columns show the results of ablation items in Table. 4.i and the ground truth.

| NIA variant  | PSNR         | SSIM          |
|--|--------------|---------------|
| a. w/o implicit body representation                    | 24.62        | 0.8888        |
| b. w/o image-based rendering                           | 24.70        | 0.9119        |
| c. w/o neural appearance blending (simple averaging)   | 25.28        | 0.9168        |
| d. w/o neural appearance blending (weighted averaging) | 25.70        | 0.9236        |
| e. full model  | <b>26.25</b> | <b>0.9268</b> |

i. NIA network components.

| # views | PSNR  | SSIM   |
|---------|-------|--------|
| 1       | 24.71 | 0.9006 |
| 2       | 25.53 | 0.9150 |
| 3       | 26.25 | 0.9268 |

ii. number of input views.

Table 4: Ablation studies on ZJU-MoCap dataset; novel view synthesis task.

from the source images (*i.e.*, image-based rendering), adaptively to different regions to render. Instead of our learnable design, we experiment by replacing it with two plausible deterministic functions. The first is a naive simple averaging of different color predictions (*c*), and the second is a weighted averaging based on the cosine similarity between each source view’s viewing direction and the target view (*d*). The comparison in rows-(*c*, *d*, *e*) verifies the benefit of our learnable appearance blender, demonstrated by the gains of +0.97 dB / +1.0% and +0.45 dB / +0.3% in PSNR and SSIM over the two deterministic variants respectively. Fig. 6 also shows the contribution of adaptive blending that helps resolving the blurs and ghosting artifacts.

**Number of camera views.** Table. 4.ii shows that the performance of our NIA gradually increases with more source views. Increasing the number of source views can provide our model with more relevant observations from the views closer to the target view.

**Visualizations.** In Fig. 6, we visualize the learned blending weight maps for all source views (#1, 2, and 3) and the color prediction from the learned implicit body representation (denoted as channel #0). Among the source views, we observe that the view #2 which is the most similar to the target view, is highly weighted in large area. Meanwhile, the implicit body representation takes charge of the overall content regions while especially highlighting the occluded regions that are not visible from all source views, (*e.g.*, the left boundary of the torso, and behind the right hand). With our neural appearance blending, our NIA is able to properly blend the available observations and the learned NeRF prediction.

## 5 CONCLUSION

We introduce Neural Image-based Avatars (NIA), a novel approach for feed-forward avatar creation from sparse view images of unseen persons. Our key idea is to learn to adaptively combine the parametric body model-based NeRF and image-based rendering techniques. Our rendering results in novel view synthesis and pose animation tasks exhibit improved robustness and fine details on different human subjects and poses. Notably, our NIA outperforms the state-of-the-art competitors, and even per-subject optimized methods in both tasks. We believe our approach is a step forward in generalizing the creation of human avatars capable of their free-view synthesis and pose animation.

## 6 ACKNOWLEDGMENTS

We thank Sida Peng of Zhejiang University for many very helpful discussions on a variety of implementation details of the Animatable-NeRF. We thank Shih-Yang Su of University of British Columbia for helpful discussions on the A-NeRF details. We thank Prof. Helge Rhodin of UBC and his group for the insightful discussions on the human performance capture. This work was partially supported by National Science Foundation Award 2107454.

## REFERENCES

- Kara-Ali Aliev, Dmitry Ulyanov, and Victor Lempitsky. Neural point-based graphics. *arXiv preprint arXiv:1906.08240*, 2(3):4, 2019.
- Timur Bagautdinov, Chenglei Wu, Tomas Simon, Fabian Prada, Takaaki Shiratori, Shih-En Wei, Weipeng Xu, Yaser Sheikh, and Jason Saragih. Driving-signal aware full-body avatars. *ACM Transactions on Graphics (TOG)*, 40(4):1–17, 2021.
- Bharat Lal Bhatnagar, Cristian Sminchisescu, Christian Theobalt, and Gerard Pons-Moll. Loopreg: Self-supervised learning of implicit surface correspondences, pose and shape for 3d human mesh registration. *Advances in Neural Information Processing Systems*, 33:12909–12922, 2020.
- Chris Buehler, Michael Bosse, Leonard McMillan, Steven Gortler, and Michael Cohen. Unstructured lumigraph rendering. In *Proceedings of the 28th annual conference on Computer graphics and interactive techniques*, pp. 425–432, 2001.
- Jianchuan Chen, Ying Zhang, Di Kang, Xuefei Zhe, Linchao Bao, Xu Jia, and Huchuan Lu. Animatable neural radiance fields from monocular rgb videos, 2021.
- Mingfei Chen, Jianfeng Zhang, Xiangyu Xu, Lijuan Liu, Jiashi Feng, and Shuicheng Yan. Geometry-guided progressive nerf for generalizable and efficient neural human rendering. *ECCV*, 2022.
- Shenchang Eric Chen and Lance Williams. View interpolation for image synthesis. In *Proceedings of the 20th annual conference on Computer graphics and interactive techniques*, pp. 279–288, 1993.
- Wei Cheng, Su Xu, Jingtan Piao, Chen Qian, Wayne Wu, Kwan-Yee Lin, and Hongsheng Li. Generalizable neural performer: Learning robust radiance fields for human novel view synthesis. *arXiv preprint arXiv:2204.11798*, 2022.
- Paul Debevec, Yizhou Yu, and George Borshukov. Efficient view-dependent image-based rendering with projective texture-mapping. In *Eurographics Workshop on Rendering Techniques*, pp. 105–116. Springer, 1998.
- Junting Dong, Qing Shuai, Yuanqing Zhang, Xian Liu, Xiaowei Zhou, and Hujun Bao. Motion capture from internet videos. In *European Conference on Computer Vision*, pp. 210–227. Springer, 2020.
- Junting Dong, Qi Fang, Wen Jiang, Yurou Yang, Hujun Bao, and Xiaowei Zhou. Fast and robust multi-person 3d pose estimation and tracking from multiple views. In *T-PAMI*, 2021.
- Qi Fang, Qing Shuai, Junting Dong, Hujun Bao, and Xiaowei Zhou. Reconstructing 3d human pose by watching humans in the mirror. In *CVPR*, 2021.
- Guy Gafni, Justus Thies, Michael Zollhofer, and Matthias Nießner. Dynamic neural radiance fields for monocular 4d facial avatar reconstruction. In *Proceedings of the IEEE/CVF Conference on Computer Vision and Pattern Recognition*, pp. 8649–8658, 2021.
- Chen Gao, Yichang Shih, Wei-Sheng Lai, Chia-Kai Liang, and Jia-Bin Huang. Portrait neural radiance fields from a single image. *arXiv preprint arXiv:2012.05903*, 2020.
- Ke Gong, Xiaodan Liang, Yicheng Li, Yimin Chen, Ming Yang, and Liang Lin. Instance-level human parsing via part grouping network. In *Proceedings of the European Conference on Computer Vision (ECCV)*, pp. 770–785, 2018.

- Steven J Gortler, Radek Grzeszczuk, Richard Szeliski, and Michael F Cohen. The lumigraph. In *Proceedings of the 23rd annual conference on Computer graphics and interactive techniques*, pp. 43–54, 1996.
- Artur Grigorev, Karim Iskakov, Anastasia Ianina, Renat Bashirov, Ilya Zakharkin, Alexander Vakhitov, and Victor Lempitsky. Stylepeople: A generative model of fullbody human avatars. In *Proceedings of the IEEE/CVF Conference on Computer Vision and Pattern Recognition*, pp. 5151–5160, 2021.
- Marc Habermann, Weipeng Xu, Michael Zollhoefer, Gerard Pons-Moll, and Christian Theobalt. Livecap: Real-time human performance capture from monocular video. *ACM Transactions On Graphics (TOG)*, 38(2):1–17, 2019.
- Marc Habermann, Weipeng Xu, Michael Zollhofer, Gerard Pons-Moll, and Christian Theobalt. Deepcap: Monocular human performance capture using weak supervision. In *Proceedings of the IEEE/CVF Conference on Computer Vision and Pattern Recognition*, pp. 5052–5063, 2020.
- Marc Habermann, Lingjie Liu, Weipeng Xu, Michael Zollhoefer, Gerard Pons-Moll, and Christian Theobalt. Real-time deep dynamic characters. *ACM Transactions on Graphics (TOG)*, 40(4):1–16, 2021.
- Tong He, Yuanlu Xu, Shunsuke Saito, Stefano Soatto, and Tony Tung. Arch++: Animation-ready clothed human reconstruction revisited. In *Proceedings of the IEEE/CVF International Conference on Computer Vision*, pp. 11046–11056, 2021.
- Peter Hedman, Julien Philip, True Price, Jan-Michael Frahm, George Drettakis, and Gabriel Brostow. Deep blending for free-viewpoint image-based rendering. *ACM Transactions on Graphics (TOG)*, 37(6):1–15, 2018.
- Zeng Huang, Yuanlu Xu, Christoph Lassner, Hao Li, and Tony Tung. Arch: Animatable reconstruction of clothed humans. In *Proceedings of the IEEE/CVF Conference on Computer Vision and Pattern Recognition*, pp. 3093–3102, 2020.
- Ladislav Kavan, Steven Collins, Jiří Žára, and Carol O’Sullivan. Skinning with dual quaternions. In *Proceedings of the 2007 symposium on Interactive 3D graphics and games*, pp. 39–46, 2007.
- Youngjoong Kwon, Stefano Petrangeli, Dahun Kim, Haoliang Wang, Henry Fuchs, and Viswanathan Swaminathan. Rotationally-consistent novel view synthesis for humans. In *Proceedings of the 28th ACM International Conference on Multimedia*, pp. 2308–2316, 2020a.
- Youngjoong Kwon, Stefano Petrangeli, Dahun Kim, Haoliang Wang, Eunbyung Park, Viswanathan Swaminathan, and Henry Fuchs. Rotationally-temporally consistent novel view synthesis of human performance video. In *European Conference on Computer Vision*, pp. 387–402. Springer, 2020b.
- Youngjoong Kwon, Dahun Kim, Duygu Ceylan, and Henry Fuchs. Neural human performer: Learning generalizable radiance fields for human performance rendering. *Advances in Neural Information Processing Systems*, 34, 2021.
- Marc Levoy and Pat Hanrahan. Light field rendering. In *Proceedings of the 23rd annual conference on Computer graphics and interactive techniques*, pp. 31–42, 1996.
- John P Lewis, Matt Cordner, and Nickson Fong. Pose space deformation: a unified approach to shape interpolation and skeleton-driven deformation. In *Proceedings of the 27th annual conference on Computer graphics and interactive techniques*, pp. 165–172, 2000.
- Baoyuan Liu, Min Wang, Hassan Foroosh, Marshall Tappen, and Marianna Pensky. Sparse convolutional neural networks. In *Proceedings of the IEEE conference on computer vision and pattern recognition*, pp. 806–814, 2015.
- Lingjie Liu, Weipeng Xu, Marc Habermann, Michael Zollhöfer, Florian Bernard, Hyeongwoo Kim, Wenping Wang, and Christian Theobalt. Neural human video rendering by learning dynamic textures and rendering-to-video translation. *arXiv preprint arXiv:2001.04947*, 2020.

- Lingjie Liu, Marc Habermann, Viktor Rudnev, Kripasindhu Sarkar, Jiatao Gu, and Christian Theobalt. Neural actor: Neural free-view synthesis of human actors with pose control. *ACM Transactions on Graphics (TOG)*, 40(6):1–16, 2021.
- Matthew Loper, Naureen Mahmood, Javier Romero, Gerard Pons-Moll, and Michael J Black. Smpl: A skinned multi-person linear model. *ACM transactions on graphics (TOG)*, 34(6):1–16, 2015.
- Marko Mihajlovic, Aayush Bansal, Michael Zollhoefer, Siyu Tang, and Shunsuke Saito. Keypointnerf: Generalizing image-based volumetric avatars using relative spatial encoding of keypoints. In *European Conference on Computer Vision (ECCV) 2022*, 2022.
- Ben Mildenhall, Pratul P Srinivasan, Matthew Tancik, Jonathan T Barron, Ravi Ramamoorthi, and Ren Ng. Nerf: Representing scenes as neural radiance fields for view synthesis. In *European Conference on Computer Vision*, pp. 405–421. Springer, 2020.
- Atsuhiro Noguchi, Xiao Sun, Stephen Lin, and Tatsuya Harada. Neural articulated radiance field. In *Proceedings of the IEEE/CVF International Conference on Computer Vision*, pp. 5762–5772, 2021.
- Keunhong Park, Utkarsh Sinha, Jonathan T Barron, Sofien Bouaziz, Dan B Goldman, Steven M Seitz, and Ricardo Martin-Brualla. Nerfies: Deformable neural radiance fields. In *Proceedings of the IEEE/CVF International Conference on Computer Vision*, pp. 5865–5874, 2021a.
- Keunhong Park, Utkarsh Sinha, Peter Hedman, Jonathan T Barron, Sofien Bouaziz, Dan B Goldman, Ricardo Martin-Brualla, and Steven M Seitz. Hypernerf: A higher-dimensional representation for topologically varying neural radiance fields. *arXiv preprint arXiv:2106.13228*, 2021b.
- Sida Peng, Junting Dong, Qianqian Wang, Shangzhan Zhang, Qing Shuai, Xiaowei Zhou, and Hujun Bao. Animatable neural radiance fields for modeling dynamic human bodies. In *ICCV*, 2021a.
- Sida Peng, Yuanqing Zhang, Yinghao Xu, Qianqian Wang, Qing Shuai, Hujun Bao, and Xiaowei Zhou. Neural body: Implicit neural representations with structured latent codes for novel view synthesis of dynamic humans. In *CVPR*, 2021b.
- Sida Peng, Shangzhan Zhang, Zhen Xu, Chen Geng, Boyi Jiang, Hujun Bao, and Xiaowei Zhou. Animatable neural implicit surfaces for creating avatars from videos. *arXiv preprint arXiv:2203.08133*, 2022.
- Albert Pumarola, Enric Corona, Gerard Pons-Moll, and Francesc Moreno-Noguer. D-nerf: Neural radiance fields for dynamic scenes. *arXiv preprint arXiv:2011.13961*, 2020.
- Amit Raj, Julian Tanke, James Hays, Minh Vo, Carsten Stoll, and Christoph Lassner. Anr: Articulated neural rendering for virtual avatars. In *Proceedings of the IEEE/CVF Conference on Computer Vision and Pattern Recognition*, pp. 3722–3731, 2021a.
- Amit Raj, Michael Zollhoefer, Tomas Simon, Jason Saragih, Shunsuke Saito, James Hays, and Stephen Lombardi. Pva: Pixel-aligned volumetric avatars. *arXiv preprint arXiv:2101.02697*, 2021b.
- Daniel Rebain, Mark Matthews, Kwang Moo Yi, Dmitry Lagun, and Andrea Tagliasacchi. Lolnerf: Learn from one look. In *Proceedings of the IEEE/CVF Conference on Computer Vision and Pattern Recognition*, pp. 1558–1567, 2022.
- Shunsuke Saito, Zeng Huang, Ryota Natsume, Shigeo Morishima, Angjoo Kanazawa, and Hao Li. Pifu: Pixel-aligned implicit function for high-resolution clothed human digitization. In *Proceedings of the IEEE/CVF International Conference on Computer Vision*, pp. 2304–2314, 2019.
- Shunsuke Saito, Tomas Simon, Jason Saragih, and Hanbyul Joo. Pifuhd: Multi-level pixel-aligned implicit function for high-resolution 3d human digitization. In *Proceedings of the IEEE/CVF Conference on Computer Vision and Pattern Recognition*, pp. 84–93, 2020.
- Katja Schwarz, Yiyi Liao, Michael Niemeyer, and Andreas Geiger. Graf: Generative radiance fields for 3d-aware image synthesis. In *Advances in Neural Information Processing Systems (NeurIPS)*, 2020.

- Shih-Yang Su, Frank Yu, Michael Zollhöfer, and Helge Rhodin. A-nerf: Articulated neural radiance fields for learning human shape, appearance, and pose. *Advances in Neural Information Processing Systems*, 34, 2021.
- Shih-Yang Su, Timur Bagautdinov, and Helge Rhodin. Danbo: Disentangled articulated neural body representations via graph neural networks. *arXiv preprint arXiv:2205.01666*, 2022.
- Justus Thies, Michael Zollhöfer, and Matthias Nießner. Deferred neural rendering: Image synthesis using neural textures. *ACM Transactions on Graphics (TOG)*, 38(4):1–12, 2019.
- Ashish Vaswani, Noam Shazeer, Niki Parmar, Jakob Uszkoreit, Llion Jones, Aidan N Gomez, Łukasz Kaiser, and Illia Polosukhin. Attention is all you need. *arXiv preprint arXiv:1706.03762*, 2017.
- Qianqian Wang, Zhicheng Wang, Kyle Genova, Pratul Srinivasan, Howard Zhou, Jonathan T Barron, Ricardo Martin-Brualla, Noah Snavely, and Thomas Funkhouser. Ibrnet: Learning multi-view image-based rendering. *arXiv preprint arXiv:2102.13090*, 2021.
- Chung-Yi Weng, Brian Curless, Pratul P Srinivasan, Jonathan T Barron, and Ira Kemelmacher-Shlizerman. Humannerf: Free-viewpoint rendering of moving people from monocular video. *arXiv preprint arXiv:2201.04127*, 2022.
- Minye Wu, Yuehao Wang, Qiang Hu, and Jingyi Yu. Multi-view neural human rendering. In *Proceedings of the IEEE/CVF Conference on Computer Vision and Pattern Recognition*, pp. 1682–1691, 2020.
- Hongyi Xu, Thiemo Alldieck, and Cristian Sminchisescu. H-nerf: Neural radiance fields for rendering and temporal reconstruction of humans in motion. *Advances in Neural Information Processing Systems*, 34, 2021.
- Alex Yu, Vickie Ye, Matthew Tancik, and Angjoo Kanazawa. pixelnerf: Neural radiance fields from one or few images. *arXiv preprint arXiv:2012.02190*, 2020.
- Fuqiang Zhao, Wei Yang, Jiakai Zhang, Pei Lin, Yingliang Zhang, Jingyi Yu, and Lan Xu. Humannerf: Efficiently generated human radiance field from sparse inputs. In *Proceedings of the IEEE/CVF Conference on Computer Vision and Pattern Recognition*, pp. 7743–7753, 2022.
- Zerong Zheng, Han Huang, Tao Yu, Hongwen Zhang, Yandong Guo, and Yebin Liu. Structured local radiance fields for human avatar modeling. *arXiv preprint arXiv:2203.14478*, 2022.

## A VIDEO RESULTS

Video results of free-viewpoint rendering, pose animation and 3D reconstruction with ZJU-MoCap and MonoCap datasets can be found at <https://youngjoongunc.github.io/nia>. We compare our NIA with IBRNet Wang et al. (2021), NHP Kwon et al. (2021), and Animatable-NeRF Peng et al. (2021a).

## B REPRODUCIBILITY

We describe the implementation details in the interest of reproducibility.

### B.1 INPUT DETAILS.

Our model requires RGB images, foreground mask, SMPL parameters, and camera calibration parameters. We compute the visibility of all SMPL vertices through rasterization using the calibration and SMPL parameters. We elaborate the used dataset details and input preparation in the Section 3.

### B.2 IMPLEMENTATION DETAILS.

**Image feature extractor.** Given  $N$  source images of shape  $H \times W$ , we use an ImageNet-pretrained ResNet-18 backbone to extract a feature pyramid. We take the multi-scale feature maps of shapes  $\{64 \times H/2 \times W/2, 64 \times H/4 \times W/4, 128 \times H/8 \times W/8, 256 \times H/16 \times W/16\}$ . These feature maps are bilinearly upsampled to the highest resolution *i.e.*,  $H/2 \times W/2$ , and concatenated into a shape  $512 \times H/2 \times W/2$ .

**Construction of the Implicit Body Representation.** As described in Section 3.1, we first define our body features anchored to the SMPL vertices by attaching the vertices’ pixel-aligned features from  $N$  source views. Since the body features, which are defined on the SMPL mesh surface, are relatively sparse in the 3D space, we cannot directly interpolate the body features corresponding to query location. Inspired by Peng et al. Peng et al. (2021b), we diffuse the body features into a volume and sample the feature at the query location. Specifically, we first compute the bounding box of the SMPL model, where the side length is enlarged by 2.5% to cover the gap between the exact human geometry and the SMPL model, and divide it with small voxel of size  $5 \times 5 \times 5 \text{ mm}^3$ . This results in the feature volume  $P_n \in \mathbb{R}^{D \times H \times W}$  (depth, height, width) for each view  $n$ . Then a series of 3D sparse convolutions Liu et al. (2015) is applied on this volume of sparse feature points (vertices) to densify them within the volume space, resulting in the output feature volume  $\tilde{P}_n \in \mathbb{R}^{\frac{P}{16} \times \frac{H}{16} \times \frac{W}{16} \times C}$ . We use  $C = 256$ . To make the feature diffusion invariant to the human position or orientation in the world coordinate system, both the body feature and query locations are transformed to the SMPL coordinate system.

Given a query point  $\mathbf{x}$ , we sample the corresponding body feature  $\mathbf{s}_n \in \mathbb{R}^C$  from the volume  $\tilde{P}_n$ . The sampled body features from  $N$  source views  $S = \{\mathbf{s}_n\}_{n=1}^N \in \mathbb{R}^{N \times C}$  are then processed by a view-wise cross-attention with the pixel-aligned features  $L = \{\mathbf{l}_n\}_{n=1}^N \in \mathbb{R}^{N \times C}$  to obtain the multi-view aware body features  $Z$  as:

$$Z = \text{softmax}\left(\frac{1}{\sqrt{d}}\phi_k(S) \cdot \phi_k(L)^T\right) \cdot \phi_v(L) + S, \quad Z = \{\mathbf{z}_n\}_{n=1}^N \in \mathbb{R}^{N \times C}, \quad (5)$$

where  $\phi_k$  and  $\phi_v$  are the key and value embedding functions as in the Transformers Vaswani et al. (2017). Besides the final density  $\sigma$  and color value  $\mathbf{c}_0$ , we also propose to predict the confidence  $\psi \in [0, 1]$  of its color prediction as:

$$\sigma = F_\sigma\left(\sum_n \mathbf{z}_n / N\right), \quad \mathbf{c}_0, \psi, \mathbf{h} = F_{\mathbf{c}_0}\left(\sum_n (\mathbf{z}_n; \gamma(d)) / N\right), \quad (6)$$

where  $F_\sigma$  and  $F_{\mathbf{c}_0}$  are MLPs consisting of four linear layers respectively, and  $\gamma : \mathbb{R}^{3 \rightarrow 6 \times l}$  is a positional encoding of viewing direction  $d \in \mathbb{R}^3$  as in Mildenhall et al. (2020) with  $2 \times l$  different basis functions.  $\mathbf{h}$  is the intermediate color feature extracted from the second to last layer of  $F_{\mathbf{c}_0}$  that is later used in the appearance blender (Section 3.2).

**Query point sampling details.** We sample the query points inside the 3D bounding box of the SMPL body with its side length enlarged by 2.5% to embrace the gap between real geometry and naked SMPL body. We sample 1024 rays, and 64 points are sampled per ray for the training. For the inference, 64 points are sampled along each ray.

**Appearance blending module.** Our appearance blending module  $F_B$  is a 8-layer MLP with ReLU activations.

### B.3 TRAINING DETAILS.

Our model is trained for 250 epochs for ZJU-MoCap. The learning rate is set to  $5 \times 10^{-4}$ . We use one RTX 3090 GPU for training, which takes 1 day.

## C DATASETS

In this section, we discuss the additional details about the datasets used, including the train/test splits and their license information. We would like to clarify that both the ZJU-Mocap and MonoCap datasets are public for research purposes and do not contain any personally identifiable information or offensive content.

### C.1 ZJU-MOCAP

ZJU-Mocap Peng et al. (2021b) is the public dataset that is available for the research and non-profit purposes only as stated in their Github page<sup>1</sup>. It provides RGB videos of 10 different human subjects captured from 23 synchronized cameras. Each video length is between 600 to 1000 frames. The ZJU-Mocap dataset provides foreground region masks computed by PGN method Gong et al. (2018), SMPL parameters fitted by EasyMocap<sup>2</sup> Dong et al. (2020); Peng et al. (2021b); Fang et al. (2021); Dong et al. (2021), and camera calibrations. We follow the training and testing protocols of NHP Kwon et al. (2021) including the data format and train/test split which are available in their Github page<sup>3</sup>.

### C.2 MONOCAP

MonoCap is the public dataset that is available for the research and non-profit purposes only as stated in their website<sup>4</sup>. MonoCap consists of DeepCap Habermann et al. (2020) and DynaCap Habermann et al. (2021) dataset sequences that are captured by dense camera views. MonoCap provides RGB images, foreground masks and camera parameters. We use EasyMocap to fit the SMPL parameters.

## D LIMITATIONS AND DISCUSSIONS

While our method offers a simple yet effective way of creating human avatars from very sparse view images, it still has a few limitations. First, it relies on accurate parametric body fitting with calibrated multi-view cameras. To democratize these human avatars, it will be worthwhile to explore directions which do not require explicit parametric model fitting. Second, the SMPL-driven deformation cannot express the complex non-rigid deformations (*e.g.*, loose clothes or garments). Also, as the target pose deviates much from the available reference pose, our pose synthesis tends to degrade. It would be an fruitful direction to find an optimal reference frame (*e.g.*, based on the similarity to a target pose). Other interesting future directions include scaling the approach to high resolution images and real-time rendering. Lastly, if the SMPL fit deviates much from the original geometry (in terms of pose or shape), the same SMPL vertex will be projected to non-corresponding pixels across different views/time. This will cause the blending of misaligned pixel colors, which in turn generates blurry results. Interesting future directions to improve the behavior are exploring the patch-wise perceptual

<sup>1</sup><https://github.com/zju3dv/neuralbody>

<sup>2</sup><https://github.com/zju3dv/EasyMocap>

<sup>3</sup>[https://github.com/YoungJoongUNC/Neural\\_Human\\_Performer](https://github.com/YoungJoongUNC/Neural_Human_Performer)

<sup>4</sup><https://gsv-assets.mpi-inf.mpg.de>

loss as in GRAF Schwarz et al. (2020) and Keypoint NeRF Mihajlovic et al. (2022) or to jointly optimize the SMPL fit.

## E SOCIETAL IMPACT

We discuss the potential societal impact of our work. The positive side of constructing an avatar from few number of cameras is that it can realize the immersive 3D teleconferencing that is affordable for most people, in contrast to earlier methods that require expensive reconstruction from dozens of cameras. Also, people can easily generate their own avatar, and explore the virtual world with it. The negative aspect is that it could be used in generating fake media, which can erode the trust against media. We strongly hope that our work can be used in positive directions.